

Joint Phase-Shift Design and Power Control for Near-and Far-Field Communications in Extremely Large RIS-aided UAV Networks

Tinh T. Bui, *Graduate Student Member, IEEE*, Dang Van Huynh, *Member, IEEE*,
Long D. Nguyen, *Member, IEEE*, Haejoon Jung, *Senior Member, IEEE*, and Trung Q. Duong, *Fellow, IEEE*

Abstract—This paper investigates the integration of drone (aka UAV)-assisted networks with a reconfigurable intelligent surface (RIS) to enhance energy efficiency in near- and far-field communication scenarios. The coexistence of near-field and far-field communications introduces unique challenges in ensuring efficient resource allocation, managing interference, and meeting quality of service requirements for users. Primary users in the near-field areas have stronger signal links, while secondary users and primary far-field users face increased path loss and interference, necessitating sophisticated optimisation strategies to balance their performance. To address these challenges, we propose a joint optimisation framework for transmission power allocation and RIS phase-shift design. The framework aims to maximise energy efficiency while maintaining reliable communication for all user groups, leveraging the complementary characteristics of UAV and RIS technologies. The low-complexity optimisation approach is developed, leveraging advanced successive convex approximation techniques and iterative algorithms. The framework consists of the Dinkelbach algorithm for the outer loop and a combination of linear and convex optimisation algorithms for the inner loop. Linear programming is employed to handle the large number of variables, such as phase-reflecting coefficients, while convex programming is used to optimise power allocation in UAVs, with convergence guaranteed. Simulation results reveal significant energy efficiency gains compared to baseline methods, demonstrating the effectiveness of the proposed framework in managing the coexistence of near- and far-field communications. The findings underscore the importance of energy-efficient design in enabling scalable and sustainable UAV-assisted networks, offering valuable insights for the development of high-performance next-generation communication systems.

Index Terms—Extremely large RIS, near-and far-field communications, UAV networks.

T. T. Bui and D. V. Huynh are with the Faculty of Engineering and Applied Science, Memorial University, St. John's, NL A1B 3X5, Canada (e-mails: {ttbui, vdhuynh}@mun.ca).

L. D. Nguyen is with Duy Tan University, Da Nang 550000, Vietnam (email: nguyendinhlong1@duytan.edu.vn).

H. Jung is with the Department of Electronics Engineering, Kyung Hee University, Yongin-si, 17104, Korea (e-mail: haejoonjung@khu.ac.kr)

T. Q. Duong is with the Faculty of Engineering and Applied Science, Memorial University, St. John's, NL A1C 5S7, Canada, and with the School of Electronics, Electrical Engineering and Computer Science, Queen's University Belfast, BT7 1NN Belfast, U.K., and also with the Department of Electronic Engineering, Kyung Hee University, Yongin-si, Gyeonggi-do 17104, South Korea (e-mail: tduong@mun.ca).

The work of T. Q. Duong was supported in part by the Canada Excellence Research Chair (CERC) Program CERC-2022-00109. The work of Haejoon Jung was supported by Institute of Information & communications Technology Planning & evaluation (IITP) grant funded by the Korea government (MSIT) (No. RS-2024-00397480, System Development of Smart Repeater in Upper-mid Band).

Corresponding authors: Trung Q. Duong and Haejoon Jung.

I. INTRODUCTION

Drone (aka UAV)-assisted communications have emerged as a promising enabler for enhancing the capacity, coverage, and efficiency of next-generation wireless networks, including the fifth generation (5G) and the sixth generation of networks. UAVs, with their high mobility and flexible deployment capabilities, can be utilised as aerial base stations, relays, or user equipment to provide seamless connectivity in diverse scenarios such as urban environments, remote areas, and emergency situations. The inherent advantages of UAVs, including their ability to establish line-of-sight (LoS) links, agile mobility, and rapid deployment, make them ideal for applications in dynamic and complex network environments [1]–[3]. These benefits are especially critical for supporting ultra-reliable low-latency communications (URLLC), massive machine-type communications (mMTC), and enhanced mobile broadband (eMBB), which are the key components of beyond 5G and 6G systems.

Despite their potentials, UAV-assisted networks also present unique challenges that demand innovative solutions. Issues such as limited energy resources, dynamic channel conditions, and efficient resource allocation remain critical barriers to their full-scale deployment. Research efforts have been directed toward addressing these challenges, including exploring clustering and reinforcement learning for resource management [4], optimising channel allocation and data delivery in cooperative communication scenarios [5], and leveraging deep reinforcement learning for resource scheduling in emergency communication networks [6]. Furthermore, energy-efficient designs for multi-UAV and vehicular network scenarios have gained attention, considering the stringent energy budgets and spectral efficiency requirements of beyond 5G systems [7], [8]. These research directions highlight the ongoing advancements and critical open problems in realising the full potential of UAV-assisted communications for future wireless networks.

The integration of UAVs with reconfigurable intelligent surface (RIS) has emerged as a promising approach to enhance the performance of next-generation wireless networks. This combination leverages the high mobility of UAVs and the wave manipulation capabilities of RIS to improve coverage, capacity, and energy efficiency (EE). Recent studies have investigated various aspects of this integration. For instance, one study explored resource allocation and three-dimensional (3D) trajectory design for power-efficient RIS-assisted UAVs

under non-orthogonal multiple access (NOMA) communications, demonstrating the potential to minimise system energy consumption through joint optimisation strategies [9]. Another research effort focused on power minimisation in RIS-assisted multi-UAV networks with NOMA, developing resource allocation schemes that jointly optimise UAV positioning, RIS reflecting coefficients, and transmit power [10]. Furthermore, investigations into UAV-assisted and RIS-supported terahertz communications highlighted the effectiveness of this integration in enhancing communication performance in the terahertz band [11]. These studies highlight the potential of UAV and RIS integration in achieving power-efficient, high-capacity, and flexible wireless communication systems, while also addressing the complex optimisation challenges involved in their deployment.

Near-field communications have gained considerable attention as a transformative technology for 6G networks, offering unique opportunities to enhance spectral efficiency, spatial resolution, and EE. Unlike traditional far-field communications, near-field communication leverages the spherical wavefront characteristics of electromagnetic waves, which become significant with extremely large-scale arrays and RIS. Recent studies have explored the fundamentals, challenges, and potentials of near-field multiple-input multiple-output (MIMO) communications, emphasising their suitability for ultra-dense networks and high-capacity systems [12]. Further advancements have investigated mixed near- and far-field communications in extremely large-scale array systems, addressing interference management and optimisation challenges in such hybrid settings [13]. Moreover, location-driven beamforming techniques for RIS-assisted near-field communications have been proposed, enabling precise control of beam directionality and significantly improving communication reliability and efficiency [14]. Additionally, research on the achievable rate optimisation of RIS-aided near-field wideband uplink systems has highlighted the critical role of RIS in expanding capacity and overcoming bandwidth limitations in near-field scenarios [15]. These advancements emphasise the significant potential of near-field communications to meet the stringent performance demands of 6G networks, while also highlighting the need for innovative solutions to tackle associated interference, beamforming, and hardware design challenges.

A. Literature Review

The integration of near- and far-field communications with extremely large RIS-aided UAV networks has been extensively studied for its potential to improve system performance in terms of capacity, spectral efficiency, and reliability. Recent research has provided key insights and solutions to address associated challenges.

Detailed near-field channel models have been introduced to characterise spherical wavefront propagation and air-ground communication effects in large-scale RIS-enabled networks. These models offer valuable insights into path loss, phase shifts, and spatial correlation, forming a basis for system-level optimisation [16]. Spatial correlation analyses for extremely large-scale array communications have provided guidelines for

designing array configurations and optimally positioning RIS elements to maximise system performance [17].

Advancements in beamforming and beam training are critical for optimising the performance of RIS-aided near-field communications. A multi-beam framework has been proposed to serve multiple users simultaneously by exploiting the spatial resolution of near-field propagation, enhancing communication efficiency through effective beam management and interference reduction [18]. Efficient codebook and beam training strategies have also been developed for RIS-aided near-field MIMO systems, addressing challenges in accurately aligning beams under near-field conditions and significantly reducing training overhead [19].

Optimising achievable rates in RIS-aided near-field communications has been a focal point, especially in wideband systems. Algorithms designed for joint optimisation of beamforming and power allocation have demonstrated significant improvements in spectral efficiency by addressing frequency-selective fading and maximising rates in wideband uplink scenarios [15]. A beamforming approach leveraging Fresnel zone characteristics has further enhanced spectral efficiency, using the unique propagation features of near-field wideband communications to support robust and high-capacity links [20].

Furthermore, the integration of UAVs with near-field communication technologies has led to significant advancements in both antenna measurement systems and mobile edge computing (MEC) networks. In MEC networks, UAVs have been utilised to enhance computational offloading in NOMA systems, particularly in scenarios where near-field and far-field communications coexist. Research has focused on optimising task offloading to minimise latency by efficiently managing communication and computing resources, such as user association, capacity allocation, and transmit power. Given the complexity of these mixed-integer programming problems, iterative algorithms employing block coordinate descent, convex transformation, and relaxation techniques have been proposed [21].

Collectively, these advancements in beamforming, rate optimisation, and channel modelling have significantly contributed to the understanding and practical implementation of near- and far-field communications in RIS-aided UAV networks, paving the way for more efficient and scalable solutions in next-generation wireless systems.

B. Motivation and Contributions

The rapid advancements in near-field communications and RIS technology have opened new possibilities for improving the performance of UAV-assisted networks, particularly in mixed primary-secondary user systems. However, significant challenges remain in integrating UAVs with RIS to address the complex requirements of serving both near-field and far-field users efficiently. Traditional approaches often focus on independent optimisation of UAV and RIS parameters, which neglects the intricate interplay between transmission power allocation and RIS phase design. Moreover, the coexistence of primary and secondary users introduces additional com-

plexities, such as interference management and ensuring EE, which are critical for sustainable network operations.

Motivated by these challenges, this paper investigates the integration of UAV-assisted networks with RIS, focusing on a scenario where primary users are served directly by UAVs, and secondary users are served by RIS. The integration of UAVs into wireless communication networks offers several key advantages. Firstly, UAVs enable dynamic eavesdropping mitigation by optimising secure communication links in real-time, adapting to potential security threats in ways stationary base stations cannot. Secondly, UAVs provide on-demand deployment, particularly beneficial in higher-frequency communications where near-field areas are wider. Their flexibility allows them to deliver high-quality service to primary near-field users while ensuring connectivity for far-field and secondary near-field users, supported by RIS. Thirdly, UAVs enhance line-of-sight communications and interference mitigation by flying at higher altitudes, increasing the likelihood of clear links. They also mitigate interference in high-frequency communications by moving to optimal locations, addressing the challenges of shorter base station distances. Finally, UAVs enable rapid deployment and scalability, making them ideal for disaster response, remote areas, or temporary events, while offering a cost-effective solution for scaling networks based on demand. Notably, the system considers near-field effects for users in primary networks and for RIS-to-secondary user links, necessitating precise modelling and optimisation techniques to fully exploit the benefits of near-field communications. The main contributions of this paper are as follows:

- We propose a practical system model for UAV-assisted networks with the support RIS that incorporates primary and secondary users. The model considers near- and far-field communication for primary users and near-field links for secondary users, capturing the unique characteristics of spherical wavefront propagation.
- To enhance the sustainability of the network, we jointly optimise transmission powers and RIS phase reflecting coefficients. The objective is to maximise EE while satisfying the quality of service (QoS) requirements for both primary and secondary users.
- We develop a comprehensive optimisation framework to tackle the formulated non-convex problem of EE maximisation. Advanced techniques, including successive convex approximation (SCA) framework and iterative algorithms, are employed to ensure computational efficiency and solution feasibility.
- Extensive simulations are conducted to evaluate the proposed optimisation framework. The results demonstrate significant improvements in EE compared to baseline methods, highlighting the effectiveness of the joint optimisation of UAV and RIS parameters in mixed near- and far-field communication environments.

By addressing the interplay between UAVs, RIS, and near-field communications in a mixed user network, this paper provides a foundation for future research and practical implementations in energy-efficient UAV-assisted systems.

C. Paper Structure and Notations

The remainder of the paper is structured as follows. Section II presents the system model and formulates the EE optimisation problem, detailing the interactions between UAVs, RIS, and users in the mixed primary-secondary network. Section III introduces the proposed solution, including the joint optimisation framework for transmission power allocation and RIS phase reflecting coefficients, alongside the algorithmic approach to solve the non-convex problem. Section IV provides simulation results, showcasing the performance of the proposed solution and comparing it with baseline methods to highlight its effectiveness in improving EE. Finally, Section V concludes the paper, summarising the key findings and discussing potential directions for future research.

The mathematical notations used in this paper are as follows. The Kronecker product is denoted by \otimes . The Euclidean norm of a vector is denoted by $\|\mathbf{x}\|$. The logarithm with base 2 is represented by $\log_2(\cdot)$, while the base 10 logarithm is denoted by $\log(\cdot)$. The function $\text{diag}(\mathbf{x})$ represents a diagonal matrix with the elements of vector \mathbf{x} on its main diagonal. For complex numbers, $\Re(\cdot)$ and $\Im(\cdot)$ denote the real and imaginary parts, respectively. The trace of a matrix \mathbf{X} is denoted by $\text{trace}(\mathbf{X})$, and the determinant is represented by $\det(\mathbf{X})$. The transpose and conjugate transpose (Hermitian) of a matrix \mathbf{X} are denoted by \mathbf{X}^T and \mathbf{X}^H , respectively. Finally, $\mathbb{E}[\cdot]$ denotes the expectation operator, and $|\cdot|$ represents the absolute value for scalars or the cardinality for sets.

II. SYSTEM MODEL AND PROBLEM FORMULATION

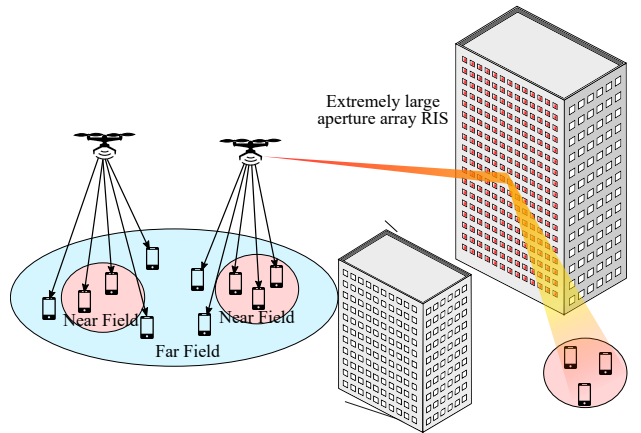


Fig. 1. An illustration of the considered system model.

The system model considers a set of UAVs, denoted as $\mathcal{U} = \{1, \dots, U\}$, each equipped with N_U antennas. Additionally, a RIS is employed, which is configured as a uniform planar array consisting of N_{R1} reflecting elements per row and N_{R2} reflecting elements per column, resulting in a total of $N_R = N_{R1} \times N_{R2}$ reflecting elements. The primary users, represented by the set $\mathcal{K} = \{1, \dots, K\}$, are directly served by the UAVs, while the secondary users, represented by the set $\mathcal{M} = \{1, \dots, M\}$, are served via the UAVs through the RIS. We assume that primary users are located in both near- and far-field areas of UAVs while secondary users are in

near-field areas of the RIS. All users are assumed to have a single omnidirectional antenna. The location of each user k , UAV, and RIS are denoted by \mathbf{q}_k , \mathbf{q}_u , and \mathbf{q}_{RIS} , respectively. Meanwhile, the positions of antenna i in the antenna array equipped in UAV u and the RIS are represented by $\mathbf{q}_{u,i}$ and $\mathbf{q}_{RIS,i}$, respectively.

A. Channel Model

Since the locations of UAVs and the RIS are in the high altitudes, the LoS paths dominate the others. Therefore, we assume that signals are transmitted directly on one path from UAVs to the RIS without any scatters, causing the channel matrix from UAV u to the RIS [22]:

$$\mathbf{H}_{u,RIS} = \sqrt{\frac{1}{\text{PL}_{u,RIS}}} \beta_{u,RIS} \mathbf{b}(\phi_u^{(in)}, \varphi_u^{(in)}) \mathbf{a}_u^H(\gamma_u) \quad (1)$$

where $\text{PL}_{u,RIS} = \left(\frac{4\pi\|\mathbf{q}_u - \mathbf{q}_{RIS,0}\|}{\lambda}\right)^2$, $\beta_{u,RIS}$ denote the path-loss and the complex gain from UAV u to the RIS, respectively. $\phi_u^{(in)}$, $\varphi_u^{(in)}$, γ_u are the azimuth angle of arrival (AoA), elevation AoA at the RIS, and the azimuth angle of departure (AoD) at UAV u , respectively. Due to far-field communication between UAVs and RIS, the far-field array steering vectors of UAV u and the RIS can be expressed respectively as follows [18]

$$\mathbf{a}_u(\gamma_u) = \frac{1}{\sqrt{N_U}} \left[e^{-j\frac{2\pi n_u d_U}{\lambda} \sin \gamma_u} \right]_{n_u=0, \dots, N_U-1}^T, \quad (2)$$

$$\begin{aligned} \mathbf{b}(\phi_u^{(in)}, \varphi_u^{(in)}) &= \frac{1}{\sqrt{N_R}} \left[e^{-j\frac{2\pi n_1 d_R}{\lambda} \sin \phi_u^{(in)} \cos \varphi_u^{(in)}} \right]_{n_1=0, N_{R1}-1}^T \\ &\otimes \left[e^{j\frac{2\pi n_2 d_R}{\lambda} \sin \varphi_u^{(in)}} \right]_{n_2=0, N_{R2}-1}^T. \end{aligned} \quad (3)$$

The distinction between near-field and far-field channel models arises from the nature of the received waveform: near-field users experience a spherical waveform, while far-field users receive a planar waveform. Consequently, the key modeling parameters differ significantly. For near-field communication, the locations of antennas are the primary focus, whereas for far-field communication, the angle of arrival becomes the central parameter.

Near- and far-field areas are commonly separated by the Rayleigh distance with the formulation as $d_R = \frac{2(N-1)^2 d^2}{\lambda}$ where N , d , and λ are the number of antennas, antenna spacing, and carrier wavelength. Channel from UAV u to far-field user k is modelled as

$$\mathbf{h}_{u,k}^{NF} = \frac{\lambda e^{-j\frac{2\pi}{\lambda}\|\mathbf{q}_k - \mathbf{q}_{u,1}\|}}{4\pi\|\mathbf{q}_k - \mathbf{q}_{u,0}\|} \left[e^{-j\frac{2\pi d_U}{\lambda} \sin \theta_{k,u}} \right]_{n=0, N_U-1}^T. \quad (4)$$

Channel from UAV u to near-field user k is modelled as

$$\mathbf{h}_{u,k}^{FF} = \frac{\lambda}{4\pi\|\mathbf{q}_k - \mathbf{q}_{u,0}\|} \left[e^{-j\frac{2\pi}{\lambda}\|\mathbf{q}_k - \mathbf{q}_{u,n}\|} \right]_{n=0, N_U-1}^T. \quad (5)$$

Channel from the RIS to near-field user m is modelled as

$$\mathbf{h}_{RIS,m}^{NF} = g_{RIS,k}^{NF} [e^{-j\frac{2\pi}{\lambda}\|\mathbf{q}_m - \mathbf{q}_{1,n_2}\|}, \dots, e^{-j\frac{2\pi}{\lambda}\|\mathbf{q}_m - \mathbf{q}_{1,N_{R2}}\|}, \dots, e^{-j\frac{2\pi}{\lambda}\|\mathbf{q}_m - \mathbf{q}_{N_{R1},1}\|}, \dots, e^{-j\frac{2\pi}{\lambda}\|\mathbf{q}_m - \mathbf{q}_{N_{R1},N_{R2}}\|}], \quad (6)$$

where the large-scale path loss $g_{RIS,k}^{NF} = \lambda/(4\pi\|\mathbf{q}_m - \mathbf{q}_{RIS,0}\|)$, $\mathbf{q}_{RIS,0}$ is the coordinate of the centre of the RIS.

B. Communication model

The received signal at primary user k which is served by UAV u can be expressed as

$$y_k = \mathbf{h}_{u,k} \mathbf{f}_{u,k} x_{u,k} + \sum_{u' \in \mathcal{U}} \sum_{k' \in \mathcal{K} \cup \mathcal{M} \setminus k} \pi_{u',k'}^{(1)} \mathbf{h}_{u',k'} \mathbf{f}_{u',k'} x_{u',k'} + n_k, \quad (7)$$

where $n_k \sim CN(0, \sigma_k^2)$ denotes the additive white Gaussian noise (AWGN) at primary user k , $x_{u,k}$ is the transmitted symbol from UAV u to user k , and $\pi_{u,k}^{(1)}$ is the association matrix for primary users to UAVs. If the value of an element $\pi_{u,k}^{(1)}$ in $\pi^{(1)}$ is 1, then UAV u serves user k , otherwise UAV u does not serve user k . Due to lower penetration capabilities of high-frequency signals through solid obstacles, we assume that there is no LoS channel from UAVs to secondary users in the remote area. The received signal at the secondary user m can be formulated as

$$y_m = \mathbf{h}_{RIS,m} \Theta \mathbf{H}_{u,RIS} \mathbf{f}_{u,m} x_{u,m} + n_m + \sum_{u' \in \mathcal{U}} \sum_{m' \in \mathcal{K} \cup \mathcal{M} \setminus m} \pi_{u',m'}^{(2)} \mathbf{h}_{u',m'} \Theta \mathbf{H}_{u',RIS} \mathbf{f}_{u',m'} x_{u',m'}, \quad (8)$$

where the diagonal matrix $\Theta = \text{diag}(\boldsymbol{\theta}) \in \mathbb{C}^{N_R \times N_R}$ represents the beamforming matrix controlled by phase reflecting coefficients, $\boldsymbol{\theta} = [e^{j\theta_1}, \dots, e^{j\theta_{N_R}}] \in \mathbb{C}^{N_R}$ is the vector consisting of reflecting coefficients with each element $\theta_i \in [0, 2\pi)$. $\pi^{(2)}$ is the association matrix for secondary users to UAVs. If the value of an element $\pi_{u,m}^{(2)}$ in $\pi^{(2)}$ is 1, then UAV u serves secondary user m , otherwise UAV u does not serve user m .

The upper bound of the data rate of primary user k can be expressed as

$$R_k = B \log_2 \left(1 + \frac{|\mathbf{h}_{u,k} \mathbf{f}_{u,k}|^2 p_{u,k}}{\sum_{\substack{u' \in \mathcal{U} \\ k' \in \mathcal{K} \cup \mathcal{M} \\ k' \neq k}} \pi_{u',k'}^{(1)} |\mathbf{h}_{u',k'} \mathbf{f}_{u',k'}|^2 p_{u',k'} + \sigma_k^2} \right). \quad (9)$$

In (9), due to the long distance between the RIS and the primary area, the interference from RIS received at primary users is minor compared to the one from UAVs. In addition, we assume that there are many obstacles between UAVs and the secondary users. Therefore, direct interference from UAVs to the secondary users is neglected. The upper bound of the data rate of secondary user m can be expressed as

$$R_m = B \log_2 \left(1 + \frac{|\mathbf{h}_{RIS,m} \Theta \mathbf{H}_{u,RIS} \mathbf{f}_{u,m}|^2 p_{u,m}}{I_m + \sigma_m^2} \right), \quad (10)$$

where $I_m = \sum_{\substack{u' \in \mathcal{U} \\ m' \in \mathcal{K} \cup \mathcal{M} \\ m' \neq m}} \pi_{u',m'}^{(2)} |\mathbf{h}_{u',m'} \Theta \mathbf{H}_{u',RIS} \mathbf{f}_{u',m'}|^2 p_{u',m'}$ is the interference received at user m .

C. Optimisation Problem Formulation

EE plays a pivotal role in the design and operation of UAV-assisted networks, particularly due to the inherent limitations in active time and battery capacity of UAVs. The finite energy reserves of UAVs impose strict constraints on their operational lifespan, making efficient energy utilisation essential to ensure sustainable and uninterrupted network performance. Moreover, as UAVs are often deployed in dynamic and resource-intensive environments, such as those involving near- and far-field communications, optimising EE becomes critical for balancing power consumption with the QoS requirements of users. In this context, investigating and enhancing EE is not only a technical necessity but also a key enabler for scalable, robust, and future-proof UAV-assisted communication systems.

The primary objective is to maximise the EE of the system, defined as the ratio of the total throughput to the total energy consumption. Mathematically, the problem is formulated as follows

$$\max_{\mathbf{P}, \Theta} \frac{\sum_{k=1}^K R_k(\mathbf{P}) + \sum_{m=1}^M R_m(\mathbf{P}, \Theta)}{UP_{cc} + \sum_{u=1}^U \left(\sum_{k=1}^K \pi_{u,k}^{(1)} P_{u,k} + \sum_{m=1}^M \pi_{u,m}^{(2)} P_{u,m} \right)} \quad (11a)$$

$$\text{s.t.} \sum_{k=1}^K \pi_{u,k}^{(1)} P_{u,k} + \sum_{m=1}^M \pi_{u,m}^{(2)} P_{u,m} \leq P_{\max}, \forall u \in \mathcal{U}, \quad (11b)$$

$$R_k(\mathbf{P}) \geq R_{\min}^{(1)}, \forall k \in \mathcal{K}, \quad (11c)$$

$$R_m(\mathbf{P}, \Theta) \geq R_{\min}^{(2)}, \forall m \in \mathcal{M}, \quad (11d)$$

$$\mathbf{P} \geq 0, \quad (11e)$$

$$0 \leq \theta_i \leq 2\pi, \forall i, \quad (11f)$$

where P_{cc} is the active circuit power of an UAV, $R_k(\mathbf{P})$ is the data rate of the primary user k , $R_m(\mathbf{P}, \Theta)$ is the data rate of the secondary user m , and $P_{u,k}$ is the transmit power of UAV u allocated to serve user k . The constraints include:

- (11b) limits the maximum transmit power of UAVs.
- (11c), (11d) guarantee the minimum data rate of primary users and secondary users, respectively.
- (11e), (11f) guarantee the values of power and phase-shift value in the feasible sets.

III. PROPOSED SOLUTION

Dinkelbach algorithm is used to transform the fractional objective function into a sequence of parameterised sub-problems as

$$\max_{\mathbf{P}, \Theta, \mu} \sum_{k=1}^K R_k(\mathbf{P}) + \sum_{m=1}^M R_m(\mathbf{P}, \Theta) - \mu L(\mathbf{P}) \quad (12a)$$

$$\text{s.t.} \quad (11b), (11c), (11d), (11e), (11f), \quad (12b)$$

where μ is the slack variable, and $L(\mathbf{P}) = UP_{cc} + \sum_{u=1}^U \left(\sum_{k=1}^K \pi_{u,k}^{(1)} P_{u,k} + \sum_{m=1}^M \pi_{u,m}^{(2)} P_{u,m} \right)$. At the iteration i , the parameter μ is updated using the formula as

$$\mu^{(i+1)} = \frac{\sum_{k=1}^K R_k(\mathbf{P}^{(i)}) + \sum_{m=1}^M R_m(\mathbf{P}^{(i)}, \Theta^{(i)})}{L(\mathbf{P}^{(i)})} \quad (13)$$

To solve problem (12), we fix the parameter μ and solve the problem using block coordinate descent (BCD). In terms of BCD approach, the original problem is divided into multiple sub-problems with multiple separated blocks of variables \mathbf{P}, Θ . The algorithm to solve problem (12) is described in Alg. 1.

Algorithm 1 Dinkelbach Algorithm

- 1: Initialize $\mu^{(0)} > 0$, $\epsilon_\mu > 0$, and set $i = 0$.
 - 2: **repeat**
 - 3: Solve the phase optimisation problem (14) and update RIS phase-shift coefficients $\Theta^{(i)}$.
 - 4: Solve the power optimisation problem (22) and update power allocation matrix $\mathbf{P}^{(i)}$.
 - 5: Update $\mu^{(i+1)}$ using (13).
 - 6: Compute the value of objective function $\phi(\mu^{(i)})$ in (12a).
 - 7: Increase $i = i + 1$.
 - 8: **until** $|\phi(\mu^{(i+1)}) - \phi(\mu^{(i)})| / |\phi(\mu^{(i)})| < \epsilon_\mu$.
-

A. RIS Phase Optimisation

To solve RIS phase optimisation, the values of power allocated at all UAVs and parameter μ are fixed. Since the variables Θ are only in the data rate of secondary users, the sub-optimisation problem can be expressed as

$$\max_{\Theta} \sum_{m=1}^M R_m(\Theta) \quad (14a)$$

$$\text{s.t.} \quad (11d), (11f). \quad (14b)$$

According to [23], we can approximate the lower bound of (14a) as

$$\begin{aligned} \frac{R_m(\Theta)}{\log_2(10)} &= \sum_k \log \left(1 + \frac{|X|^2}{Y} \right) \geq \frac{\tilde{R}_m(\theta; \theta)}{\log_2(10)} \\ &\triangleq -\frac{|X|^2}{\underline{Y}(\underline{Y} + |X|^2)} Y + 2\Re \left(\frac{|X|^2 X}{\underline{Y} X} \right) \\ &\quad + \log \left(1 + \frac{|X|^2}{\underline{Y}} \right) - \frac{|X|^2}{\underline{Y}} - \frac{|X|^2}{\underline{Y}(\underline{Y} + |X|^2)} |X|^2, \end{aligned} \quad (15)$$

where \underline{X} and \underline{Y} are the values from the previous iteration in terms of θ and are expressed as

$$\underline{X} = \sqrt{p_{u,m}} \mathbf{f}_{u,m}^H \mathbf{H}_{u,\text{RIS}}^H \text{diag}(\mathbf{h}_{\text{RIS},m})^* \theta^H, \quad \underline{Y} = I_m(\theta) + \sigma_m^2.$$

The expressions of X and Y at the current iteration in terms of θ are defined as

$$X = \sqrt{p_{u,m}} \mathbf{f}_{u,m}^H \mathbf{H}_{u,\text{RIS}}^H \text{diag}(\mathbf{h}_{\text{RIS},m})^* \theta^H, \quad Y = \tilde{I}_m(\theta) + \sigma_m^2,$$

where $\tilde{I}_m(\boldsymbol{\theta}) \geq I_m(\boldsymbol{\theta})$. To find the upper bound of $\tilde{I}_m(\boldsymbol{\theta})$, a tight inequality is used. The interference at secondary user m can be rewritten as

$$I_m(\boldsymbol{\theta}) = \sum_{\substack{u' \in \mathcal{U} \\ m' \in \mathcal{K} \cup \mathcal{M} \\ m' \neq m}} \pi_{u',m'}^{(2)} p_{u',m'} \boldsymbol{\theta} \Upsilon_{u',m'} \boldsymbol{\theta}^H, \quad (16)$$

where $\Upsilon_{u',m'} = \text{diag}(\mathbf{h}_{\text{RIS},m}) \mathbf{H}_{u',\text{RIS}} \mathbf{f}_{u',m'} \mathbf{f}_{u',m'}^H \mathbf{H}_{u',\text{RIS}}^H \text{diag}(\mathbf{h}_{\text{RIS},m})^*$. According to [23], given two matrices $\Upsilon_{u',m'}$, $\Xi_{u',m'}$ ($\Xi_{u',m'} \succeq \Upsilon_{u',m'}$), $\Upsilon_{u',m'} = \xi_{u',m'} \xi_{u',m'}^H$, $\Xi_{u',m'} = \|\xi_{u',m'}\|_2^2 \mathbf{I}$ where $\xi_{u',m'} = \text{diag}(\mathbf{h}_{\text{RIS},m}) \mathbf{H}_{u',\text{RIS}} \mathbf{f}_{u',m'}$. An true inequation is expressed as follows

$$\begin{aligned} \boldsymbol{\theta}^H \Upsilon_{u',m'} \boldsymbol{\theta} &\leq \boldsymbol{\theta}^H \Xi_{u',m'} \boldsymbol{\theta} + 2\Re \left(\boldsymbol{\theta}^H (\Upsilon_{u',m'} - \Xi_{u',m'}) \boldsymbol{\theta} \right) \\ &+ \boldsymbol{\theta}^H (\Upsilon_{u',m'} - \Xi_{u',m'}) \boldsymbol{\theta}. \end{aligned} \quad (17)$$

Inequation (17) can be rewritten as

$$\begin{aligned} \boldsymbol{\theta} \Upsilon_{u',m'} \boldsymbol{\theta}^H &\leq \boldsymbol{\theta} \|\xi_{u',m'}\|_2^2 \mathbf{I} \boldsymbol{\theta}^H + 2\Re \left(\boldsymbol{\theta} (\Upsilon_{u',m'} \right. \\ &\left. - \|\xi_{u',m'}\|_2^2 \mathbf{I}) \boldsymbol{\theta}^H \right) + \boldsymbol{\theta} (\Upsilon_{u',m'} - \|\xi_{u',m'}\|_2^2 \mathbf{I}) \boldsymbol{\theta}^H \end{aligned} \quad (18)$$

We have $|\boldsymbol{\theta}_i| = 1, \forall i = 1, \dots, N$ and $\|\xi_{u',m'}\|_2^2 = \xi_{u',m'} \xi_{u',m'}^H = \text{trace}(\xi_{u',m'} \xi_{u',m'}^H) = \text{trace}(\Upsilon_{u',m'}) = \eta_{u',m'}$. Therefore, the non-concave expression $\boldsymbol{\theta} \Upsilon_{u',m'} \boldsymbol{\theta}^H$ has the linear upper bound expressed as

$$\begin{aligned} \boldsymbol{\theta} \Upsilon_{u',m'} \boldsymbol{\theta}^H &\leq \eta_{u',m'} + 2\Re \left(\boldsymbol{\theta} (\Upsilon_{u',m'} - \eta_{u',m'} \mathbf{I}) \boldsymbol{\theta}^H \right) \\ &+ \boldsymbol{\theta} (\Upsilon_{u',m'} - \eta_{u',m'} \mathbf{I}) \boldsymbol{\theta}^H \end{aligned} \quad (19)$$

The upper bound of interference to secondary user m can be expressed as follows

$$\begin{aligned} \tilde{I}_m(\boldsymbol{\theta}) &\triangleq \sum_{\substack{u' \in \mathcal{U} \\ m' \in \mathcal{K} \cup \mathcal{M} \\ m' \neq m}} \pi_{u',m'}^{(2)} p_{u',m'} \left[\eta_{u',m'} \right. \\ &\left. + 2\Re \left(\boldsymbol{\theta} (\Upsilon_{u',m'} - \eta_{u',m'} \mathbf{I}) \boldsymbol{\theta}^H \right) + \boldsymbol{\theta} (\Upsilon_{u',m'} - \eta_{u',m'} \mathbf{I}) \boldsymbol{\theta}^H \right], \end{aligned} \quad (20)$$

Overall, after using approximations (15) and (19), we successfully convert non-convex problem (14) into linear optimisation problem that is given as

$$\max_{\boldsymbol{\theta}} \sum_{m=1}^M \tilde{R}_m(\boldsymbol{\theta}; \boldsymbol{\theta}) \quad (21a)$$

$$\text{s.t. } \tilde{R}_m(\boldsymbol{\theta}; \boldsymbol{\theta}) \geq R_{\min}^{(2)}, \forall m \in \mathcal{M}, \quad (21b)$$

$$0 \leq \theta_i \leq 2\pi, \forall i \quad (21c)$$

Theorem 1: The optimal value in iterations for RIS phase optimisation is a monotonic increasing function. The convergence of inner loop for solving problem (14) is guaranteed.

Proof: The proof is deferred to Appendix A. ■

For complexity analysis, problem (21) has N_R complex variables and $M + 2N_R$ linear constraints. The computational complexity for solving problem (21) can be expressed as $\mathcal{O}((M + 4N_R)^{3.5} \mathcal{L})$ if using interior-point methods where \mathcal{L}

represents the number of bits required to encode the numerical data of the problem. Compared to other convex programming, the linear expressions in problems have the mathematical formulation and computational handling which can be solved solve highly efficient solvers.

B. Power Optimisation

To solve power allocation optimisation, the phase-shift coefficients of the RIS and parameter μ are fixed. The sub-optimisation problem can be expressed as

$$\max_{\mathbf{P}} \sum_{k=1}^K R_k(\mathbf{P}) + \sum_{m=1}^M R_m(\mathbf{P}) - \mu L(\mathbf{P}) \quad (22a)$$

$$\text{s.t. } (11b), (11c), (11d), (11e). \quad (22b)$$

The problem (22) is a non-convex problem due to $R_k(\mathbf{P})$ and $R_m(\mathbf{P})$. According to [24], the data rate of primary user k in the current iteration can be approximated as

$$\frac{R_k(\mathbf{P})}{B} = \log_2 \left(1 + \frac{X_k}{Y_k} \right) \geq \frac{\hat{R}_m(\mathbf{P}; \bar{\mathbf{P}})}{B} \triangleq \bar{a} - \frac{\bar{b}}{X_k} - \bar{c} Y_k, \quad (23)$$

where

$$\bar{a} = \log_2 \left(1 + \frac{\bar{X}_k}{\bar{Y}_k} \right) + \frac{2\bar{X}_k}{\ln(2)(\bar{X}_k + \bar{Y}_k)} > 0,$$

$$\bar{b} = \frac{\bar{X}_k^2}{\ln(2)(\bar{X}_k + \bar{Y}_k)} > 0,$$

$$\bar{c} = \frac{\bar{X}_k}{\ln(2)(\bar{X}_k + \bar{Y}_k)\bar{Y}_k} > 0.$$

$$X_k = |\mathbf{h}_{u,k} \mathbf{f}_{u,k}|^2 p_{u,k},$$

$$\bar{X}_k = |\mathbf{h}_{u,k} \mathbf{f}_{u,k}|^2 \bar{p}_{u,k},$$

$$Y_k = \sum_{\substack{u' \in \mathcal{U} \\ k' \in \mathcal{K} \cup \mathcal{M} \\ k' \neq k}} \pi_{u',k'}^{(1)} |\mathbf{h}_{u',k} \mathbf{f}_{u',k'}|^2 p_{u',k'} + \sigma_k^2,$$

$$\bar{Y}_k = \sum_{\substack{u' \in \mathcal{U} \\ k' \in \mathcal{K} \cup \mathcal{M} \\ k' \neq k}} \pi_{u',k'}^{(1)} |\mathbf{h}_{u',k} \mathbf{f}_{u',k'}|^2 \bar{p}_{u',k'} + \sigma_k^2.$$

The value of any $\bar{p}_{u',k'}$ is given in the previous iteration. Using the same technique in inequation (23) to approximate $R_m(\mathbf{P})$ by its lower bound $\hat{R}_m(\mathbf{P}; \bar{\mathbf{P}})$, we can successfully convert non-convex problem (22) to convex one. CVXPY in PYTHON can be effectively used to solve these convex problems. The convex problem at an iteration can be expressed as

$$\max_{\mathbf{P}} \sum_{k=1}^K \hat{R}_k(\mathbf{P}) + \sum_{m=1}^M \hat{R}_m(\mathbf{P}) - \mu L(\mathbf{P}) \quad (24a)$$

$$\text{s.t. } (11b), (11e), \quad (24b)$$

$$\hat{R}_k(\mathbf{P}) \geq R_{\min}^{(1)}, \forall k \in \mathcal{K}, \quad (24c)$$

$$\hat{R}_m(\mathbf{P}) \geq R_{\min}^{(2)}, \forall m \in \mathcal{M}, \quad (24d)$$

Theorem 2: The optimal value in iterations for power optimisation is a monotonic increasing function. The convergence of inner loop for solving problem (22) is guaranteed.

Proof: The proof is deferred to Appendix B. ■

For complexity analysis, problem (24) has $K + M$ real variables and $2K + 2M + U$ constraints. The computational complexity for solving problem (24) can be expressed as $\mathcal{O}((K + M)^2 \sqrt{2K + 2M + U})$ [25].

IV. SIMULATION RESULTS

The simulation setup is a network configuration consisting of four UAVs, each equipped with 128 antennas, operating at an altitude of 75 meters. A RIS with 128 antennas is also deployed at an altitude of 5 meters. Operating at a carrier frequency of 28 GHz, the wavelength is approximately 0.0107 meters, and the antenna spacing for both UAVs and the RIS is set to half the wavelength, approximately 0.00535 meters [21]. The Rayleigh distances for the UAVs and RIS are determined using their respective configurations based on antenna spacing and wavelength. The primary user area is centered at $(-500, 0, 0)$ with a radius of 100 meters for the coverage of each UAV, while the secondary user area is centered at

$$\left(40, -\sqrt{d_{\text{Rayleigh}}^{\text{RIS}^2} - 5^2}/2, 0\right).$$

Fig. 2 shows an example of RIS-aided UAV networks. UAVs are capable of transmitting at a maximum power of 1 W, with circuit power consumption set to 20% of the maximum transmit power. The minimum required data rates are 1 Mbps/Hz for primary users and 0.5 Mbps/Hz for secondary users. Performance evaluation is conducted over 1000 correlation times.

To solve the optimisation problems and implement the simulations, CVXPY and Python are utilised. The simulations are performed on a computing platform with a 2.1 GHz CPU and 16 GB of RAM, ensuring robust computational capacity for solving complex optimization tasks and conducting detailed evaluations. The key parameters used in the simulations are listed in Table I.

A. Convergence Speed of Optimisation Methods

Fig. 3 illustrates the convergence performance of the Dinkelbach algorithm, showing its ability to rapidly achieve near-optimal EE within the first three iterations. After an initial improvement, the EE stabilises, demonstrating the algorithm's efficiency and reliability in reaching and maintaining an optimal solution. Its swift convergence and low computational overhead make it particularly suitable for real-time applications in wireless communication networks, where efficient and timely resource allocation is critical.

Fig. 4 illustrates the convergence of the phase-shift optimisation algorithm for the RIS. The algorithm demonstrates a steady and smooth increase in the objective value, reaching near-optimal performance within approximately 10 iterations. The gradual improvement and eventual stabilisation highlight the robustness of the algorithm in solving the phase

TABLE I
SIMULATION PARAMETERS

Parameter	Value
Number of UAVs	4
Number of antennas (UAV)	128
Number of antennas (RIS)	128
UAV altitude	75 m
IRS altitude	5 m
Carrier frequency	28 GHz
Wavelength	$\frac{3 \times 10^8}{28 \times 10^9} \approx 0.0107$ m
Antenna spacing (UAV and RIS)	$\lambda/2 \approx 0.00535$ m
Rayleigh distance (UAV)	$2((128 - 1) \times 0.00535)^2/\lambda$
Rayleigh distance (RIS)	$2((128 - 1) \times 0.00535)^2/\lambda$
Primary user area center	$(-500, 0, 0)$
Primary user area radius	100 m
Secondary user area center	$(40, -\sqrt{d_{\text{Ray}}^{\text{RIS}^2} - 5^2}/2, 0)$
Number of correlation times	10
Bandwidth	10 MHz
Noise variance	-174 dBm/Hz
Maximum UAV transmit power	1 W
Circuit power	20% P_{max} W
Minimum rate for primary users, $R_{\text{min}}^{(1)}$	1 Mbps/Hz
Minimum rate for secondary users, $R_{\text{min}}^{(2)}$	0.5 Mbps/Hz

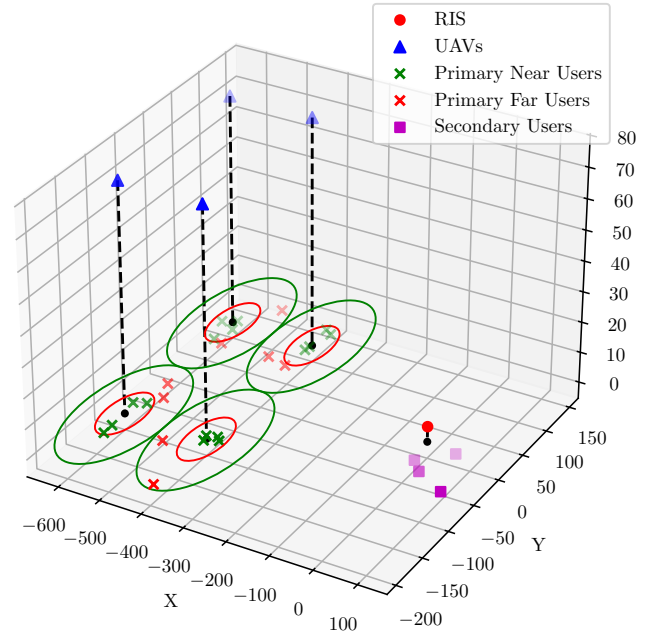


Fig. 2. An example of RIS-aided UAV networks.

optimisation problem efficiently. The convergence behaviour indicates that the algorithm effectively fine-tunes the phase shifts of the RIS to maximise the overall system performance. Additionally, Fig. 5 depicts the convergence of the power allocation optimisation algorithm for the UAVs. This algorithm converges more rapidly compared to the phase-shift optimisation, achieving near-optimal values within the first 5 iterations. The sharp initial increase in the objective value showcases the algorithm's ability to quickly identify optimal power allocation strategies, followed by stabilisation as it fine-tunes the solution. The convergence behaviours of both algorithms reflect their complementary roles in guaranteeing the convergence

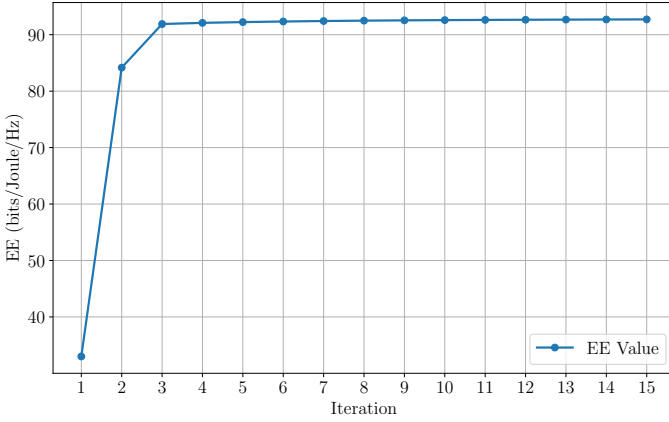


Fig. 3. Convergence speed of the Dinkelbach algorithm.

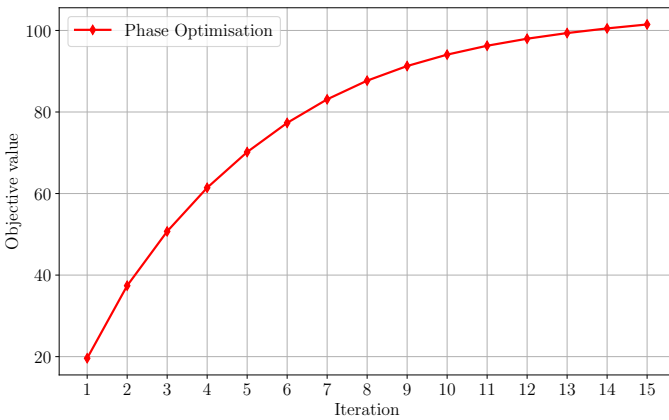


Fig. 4. Convergence speed of phase-shift optimisation algorithm.

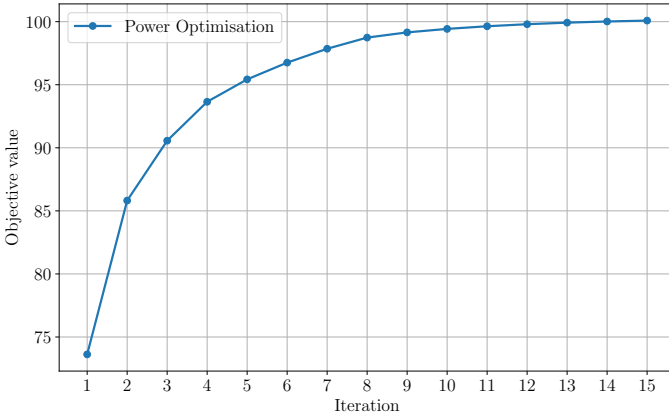


Fig. 5. Convergence speed of optimisation algorithm for power allocation.

of Dinkelbach framework. The power allocation algorithm's faster convergence supports real-time adaptability, while the phase-shift optimisation ensures fine-grained control of RIS parameters for sustained performance improvements. Overall, these algorithms ensure the overall efficiency and practicality of the proposed optimisation framework in complex communication networks.

B. Performance Analysis

To evaluate the performance of the proposed method, EEPOPA (EE maximisation through phase optimisation and power allocation), we compare it against three benchmarks. The first benchmark, EERPPA, employs random phase shifts while using power optimisation. The second, EEPORP, utilises phase optimisation combined with random power allocation. Lastly, EERPRP applies a fully randomised approach with both random phase shifts and random power allocation. These benchmarks are designed to assess the individual contributions of phase optimisation and power allocation to the overall system performance.

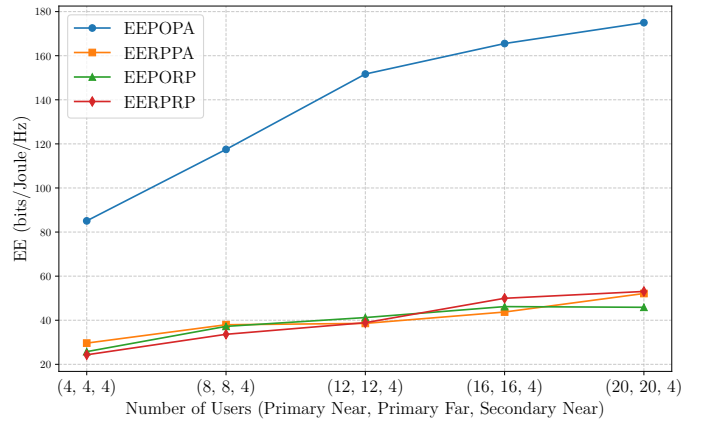


Fig. 6. The comparison in the total EE with different number of primary users.

Fig. 6 shows the EE performance of the proposed method, EEPOPA, compared to the three benchmarks as the number of users increases. In the simulation, the number of primary near users and primary far users increases simultaneously, starting from 4 users each and scaling up to 20 users each, while the number of secondary users remains constant at 4. EEPOPA consistently outperforms the benchmarks across all user configurations, with a significant margin. This highlights the effectiveness of jointly optimising phase shifts and power allocation. EERPPA, EEPORP, and EERPRP achieve much lower EE, demonstrating the limitations of randomised phase shifts or power allocation. Among the benchmarks, EERPPA shows slightly better performance, suggesting that power optimisation has a greater impact on EE compared to phase optimisation alone. The results validate the superiority of the proposed method in maximising EE, particularly as the network scales with more users. This underscores its practical applicability for energy-efficient communication in ultra-dense networks.

Fig. 7 presents the EE performance of the proposed method, EEPOPA, compared to three benchmarks—EERPPA, EEPORP, and EERPRP—as the number of secondary near users increases. The configuration begins with 4 secondary near users and scales up to 20, while the number of primary near and primary far users remains constant at 8 each. The proposed method, EEPOPA, consistently achieves the highest EE across all configurations, demonstrating its robustness and efficiency in adapting to changes in the number of secondary

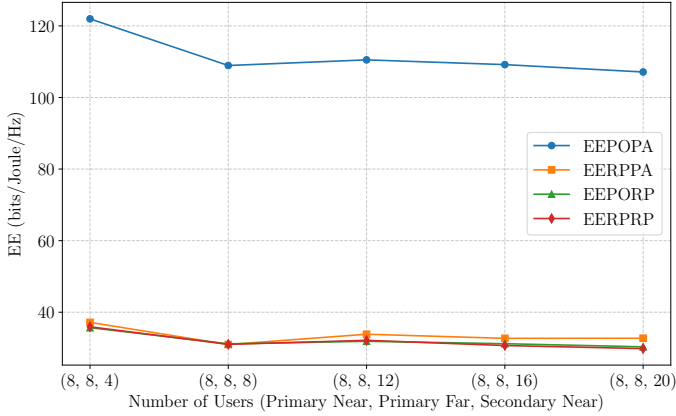


Fig. 7. The comparison in the total EE with different number of secondary users.

users. However, as the number of secondary near users increases, a slight decline in EE is observed for EEPOPA, which can be attributed to the additional resource demands introduced by the growing number of users. In contrast, the benchmarks—EERPPA, EEPORP, and EERPRP—show significantly lower EE, with minimal variation across user configurations. This suggests that the randomised approaches employed in the benchmarks fail to efficiently handle the additional complexity caused by an increasing number of secondary near users. Notably, EEPOPA exhibits a stable and scalable performance even as the number of secondary users increases, reinforcing its suitability for ultra-dense networks where secondary users play a key role. The figure also highlights the superiority of joint phase and power optimisation over partial or randomised approaches in ensuring high EE under varying user densities.

C. The Comparison of The EE Between Primary Near- and Far-field Users

The purpose of this simulation is to investigate the EE performance of primary near and primary far users under the proposed method as the number of users increases. By analysing how EE changes with varying numbers of users, we can evaluate the scalability and effectiveness of the proposed method in managing resource allocation for users at different proximities to the base station.

Fig. 8 illustrates the EE performance of primary near and primary far users as the number of primary users increases simultaneously, starting from 4 users each and scaling up to 20 users each, while the number of secondary users remains constant at 4. The results clearly show that the EE of both user groups improves as the number of users increases. The total EE for primary near users (EE_{near}) consistently outperforms the total EE for primary far users (EE_{far}) across all scenarios. For example, in the initial configuration (4, 4, 4), $EE_{\text{near}} = 44.39$ bits/Joule/Hz and $EE_{\text{far}} = 41.83$ bits/Joule/Hz. As the user count increases to (20, 20, 4), these values rise to $EE_{\text{near}} = 120.20$ bits/Joule/Hz and $EE_{\text{far}} = 82.08$ bits/Joule/Hz, respectively. This consistent gap between EE_{near} and EE_{far} highlights the impact of user

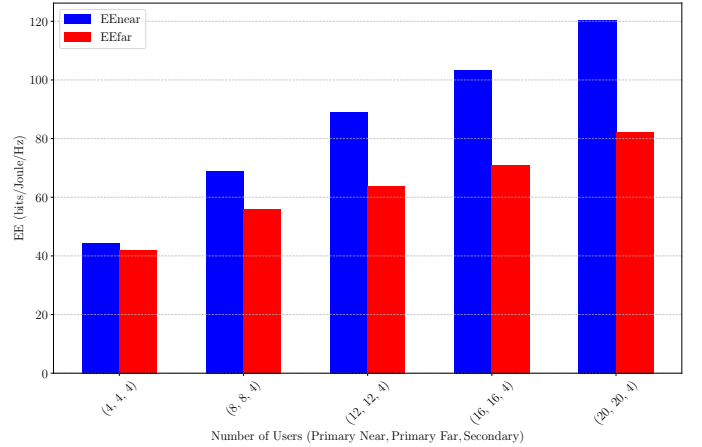


Fig. 8. EE far near bar chart.

proximity to the base station, with near users benefiting more from the optimised resource allocation. Moreover, the gradual increase in EE for both groups reflects the scalability of the proposed method in handling larger user densities. The higher growth rate in EE_{near} compared to EE_{far} further underscores the method's ability to prioritise EE for users closer to the base station, ensuring better performance in ultra-dense networks. These results validate the efficacy of the proposed method in managing EE for primary users, regardless of their proximity to the base station.

V. CONCLUSIONS

This paper has investigated the integration of UAV-assisted networks with RIS in a mixed primary-secondary user environment, focusing on enhancing EE. The proposed system model has accounted for near-field communications for certain primary users and RIS-to-secondary user links, reflecting the specific characteristics of these communication scenarios. By jointly optimising transmission powers and RIS phase reflecting coefficients, an advanced optimisation framework has been developed to maximise EE while ensuring the QoS requirements of both primary and secondary users. Due to a ultra high number of variables of phase reflecting coefficients, linear programming is employed for phase-shift design and low-complex convex programming is applied to solve power allocation for UAVs. Simulation results have demonstrated that the proposed method significantly outperforms baseline approaches in terms of EE. The results reveal consistent gains for both primary near and far users, with near users achieving higher EE due to their closer proximity to the base station. Additionally, the proposed method exhibits scalability and robustness as the number of users increases, maintaining superior EE performance compared to benchmarks. The fast convergence of the optimisation algorithms further demonstrates the practicality of the proposed solution in real-world deployments. These findings underscore the potential of combining UAVs and RIS to address the challenges of mixed near- and far-field communication scenarios in energy-efficient networks. Future research could explore extending the model to dynamic multi-UAV deployments, incorporating mobility

management and real-time adaptation to user demands, thereby advancing the capabilities of energy-efficient next-generation communication networks.

APPENDIX A
PROVING THE CONVERGENCE OF RIS PHASE
OPTIMISATION

Lets $\boldsymbol{\theta}^{(\kappa)}$, $\boldsymbol{\theta}^{(\kappa+1)}$ be the solutions of problem (21) in the $(\kappa - 1)$ -th and the κ -th loops respectively, we have

$$\tilde{R}_m(\boldsymbol{\theta}^{(\kappa+1)}; \boldsymbol{\theta}^{(\kappa)}) \geq \tilde{R}_m(\boldsymbol{\theta}^{(\kappa)}; \boldsymbol{\theta}^{(\kappa)}). \quad (25)$$

In (15), the equality holds true if $\boldsymbol{\theta} = \underline{\boldsymbol{\theta}}$. Therefore,

$$\tilde{R}_m(\boldsymbol{\theta}^{(\kappa)}; \boldsymbol{\theta}^{(\kappa)}) = R_m(\boldsymbol{\theta}^{(\kappa)}). \quad (26)$$

Also, according to (15), we have

$$R_m(\boldsymbol{\theta}^{(\kappa+1)}) \geq \tilde{R}_m(\boldsymbol{\theta}^{(\kappa+1)}; \boldsymbol{\theta}^{(\kappa)}). \quad (27)$$

Combining (25), (26), and (27), we got

$$\sum_{m=1}^M R_m(\boldsymbol{\theta}^{(\kappa+1)}) \geq \sum_{m=1}^M R_m(\boldsymbol{\theta}^{(\kappa)}), \quad (28)$$

with the convergence state is achieved when $\boldsymbol{\theta}^{(\kappa+1)} = \boldsymbol{\theta}^{(\kappa)}$. Therefore, the inner iterative algorithm for finding the solution of problem (14) is converged to a location maximum. ■

APPENDIX B
PROVING THE CONVERGENCE OF POWER OPTIMISATION

Lets $\mathbf{P}^{(\kappa)}$, $\mathbf{P}^{(\kappa+1)}$ be the solutions of problem (24) in the $(\kappa - 1)$ -th and the κ -th loops respectively. According to (23), we have

$$R_k(\mathbf{P}^{(\kappa+1)}) \geq \hat{R}_k(\mathbf{P}^{(\kappa+1)}; \mathbf{P}^{(\kappa)}) \geq \hat{R}_k(\mathbf{P}^{(\kappa)}; \mathbf{P}^{(\kappa)}) = R_k(\mathbf{P}^{(\kappa)}), \quad (29)$$

$$R_m(\mathbf{P}^{(\kappa+1)}) \geq \hat{R}_m(\mathbf{P}^{(\kappa+1)}; \mathbf{P}^{(\kappa)}) \geq \hat{R}_m(\mathbf{P}^{(\kappa)}; \mathbf{P}^{(\kappa)}) = R_m(\mathbf{P}^{(\kappa)}), \quad (30)$$

Combining (29) and (30), we got

$$\begin{aligned} & \sum_{k=1}^K \hat{R}_k(\mathbf{P}^{(\kappa+1)}) + \sum_{m=1}^M \hat{R}_m(\mathbf{P}^{(\kappa+1)}) - \mu L(\mathbf{P}^{(\kappa+1)}) \\ & \geq \sum_{k=1}^K \hat{R}_k(\mathbf{P}^{(\kappa)}) + \sum_{m=1}^M \hat{R}_m(\mathbf{P}^{(\kappa)}) - \mu L(\mathbf{P}^{(\kappa)}) \end{aligned} \quad (31)$$

Therefore, the inner iterative algorithm for finding the solution of problem (22) is converged to a location maximum. ■

APPENDIX C
PROVING THE CONVERGENCE OF DINKELBACH
ALGORITHM

Since the objective values of the inner iterative algorithms for solving problem (14) and (22) both increase monotonically. Therefore, after each outer loop, we have

$$\begin{aligned} & \sum_{k=1}^K R_k(\mathbf{P}^{(i)}) + \sum_{m=1}^M R_m(\mathbf{P}^{(i)}, \boldsymbol{\Theta}^{(i)}) - \mu^{(i)} L(\mathbf{P}^{(i)}) \geq \\ & \sum_{k=1}^K R_k(\mathbf{P}^{(i-1)}) + \sum_{m=1}^M R_m(\mathbf{P}^{(i-1)}, \boldsymbol{\Theta}^{(i-1)}) - \mu^{(i)} L(\mathbf{P}^{(i-1)}) \end{aligned} \quad (32)$$

By substituting $\mu^{(i)} = \frac{\sum_{k=1}^K R_k(\mathbf{P}^{(i-1)}) + \sum_{m=1}^M R_m(\mathbf{P}^{(i-1)}, \boldsymbol{\Theta}^{(i-1)})}{L(\mathbf{P}^{(i-1)})}$, we obtain

$$\begin{aligned} \mu^{(i+1)} &= \frac{\sum_{k=1}^K R_k(\mathbf{P}^{(i)}) + \sum_{m=1}^M R_m(\mathbf{P}^{(i)}, \boldsymbol{\Theta}^{(i)})}{L(\mathbf{P}^{(i)})} \geq \\ & \frac{\sum_{k=1}^K R_k(\mathbf{P}^{(i-1)}) + \sum_{m=1}^M R_m(\mathbf{P}^{(i-1)}, \boldsymbol{\Theta}^{(i-1)})}{L(\mathbf{P}^{(i-1)})} = \mu^{(i)} \end{aligned} \quad (33)$$

The sequence $\mu^{(i)}$ is monotonically increasing and bounded above by an optimal value μ^* . ■

REFERENCES

- [1] M. Mozaffari, W. Saad, M. Bennis, Y.-H. Nam, and M. Debbah, "A tutorial on UAVs for wireless networks: Applications, challenges, and open problems," *IEEE Commun. Surveys Tuts.*, vol. 21, no. 3, pp. 2334–2360, Sep. 2019.
- [2] M. Dai, N. Huang, Y. Wu, J. Gao, and Z. Su, "Unmanned-aerial-vehicle-assisted wireless networks: Advancements, challenges, and solutions," *IEEE Internet of Things J.*, vol. 10, no. 5, pp. 4117–4147, May 2023.
- [3] T. Do-Duy, L. D. Nguyen, T. Q. Duong, S. R. Khosravirad, and H. Claussen, "Joint optimisation of real-time deployment and resource allocation for UAV-aided disaster emergency communications," *IEEE J. Sel. Areas Commun.*, vol. 39, no. 11, pp. 3411–3424, 2021.
- [4] S. Zhou, Y. Cheng, X. Lei, Q. Peng, J. Wang, and S. Li, "Resource allocation in uav-assisted networks: A clustering-aided reinforcement learning approach," *IEEE Trans. Veh. Technol.*, vol. 71, no. 11, pp. 12 088–12 103, Nov. 2022.
- [5] M. Dai, T. H. Luan, Z. Su, N. Zhang, Q. Xu, and R. Li, "Joint channel allocation and data delivery for UAV-assisted cooperative transportation communications in post-disaster networks," *IEEE Trans. Intell. Transp. Syst.*, vol. 23, no. 9, pp. 16 676–16 689, Sep. 2022.
- [6] C. Wang, D. Deng, L. Xu, and W. Wang, "Resource scheduling based on deep reinforcement learning in UAV-assisted emergency communication networks," *IEEE Trans. Commun.*, vol. 70, no. 6, pp. 3834–3848, Jun. 2022.
- [7] N. N. Ei, M. Alsenwi, Y. K. Tun, Z. Han, and C. S. Hong, "Energy-efficient resource allocation in multi-UAV-assisted two-stage edge computing for beyond 5G networks," *IEEE Trans. Intell. Transp. Syst.*, vol. 23, no. 9, pp. 16 421–16 432, Sep. 2022.
- [8] W. Qi, Q. Song, L. Guo, and A. Jamalipour, "Energy-efficient resource allocation for UAV-assisted vehicular networks with spectrum sharing," *IEEE Trans. Veh. Technol.*, vol. 71, no. 7, pp. 7691–7702, Jul. 2022.
- [9] Y. Cai, Z. Wei, S. Hu, C. Liu, D. W. K. Ng, and J. Yuan, "Resource allocation and 3D trajectory design for power-efficient IRS-assisted UAV-NOMA communications," *IEEE Trans. Wireless Commun.*, vol. 21, no. 12, pp. 10 315–10 334, Dec. 2022.
- [10] W. Feng, J. Tang, Q. Wu, Y. Fu, X. Zhang, D. K. C. So, and K.-K. Wong, "Resource allocation for power minimization in RIS-assisted multi-UAV networks with NOMA," *IEEE Trans. Commun.*, vol. 71, no. 11, pp. 6662–6676, Nov. 2023.
- [11] Y. Pan, K. Wang, C. Pan, H. Zhu, and J. Wang, "UAV-assisted and intelligent reflecting surfaces-supported terahertz communications," *IEEE Wireless Communications Letters*, vol. 10, no. 6, pp. 1256–1260, 2021.
- [12] M. Cui, Z. Wu, Y. Lu, X. Wei, and L. Dai, "Near-field MIMO communications for 6G: Fundamentals, challenges, potentials, and future directions," *IEEE Commun. Mag.*, vol. 61, no. 1, pp. 40–46, Jan. 2023.

- [13] Y. Zhang, C. You, L. Chen, and B. Zheng, "Mixed near- and far-field communications for extremely large-scale array: An interference perspective," *IEEE Commun. Lett.*, vol. 27, no. 9, pp. 2496–2500, Sep. 2023.
- [14] X. Zheng, W. Cheng, J. Wang, and W. Zhang, "Location-driven beamforming for RIS-assisted near-field communications," *IEEE Commun. Mag.*, vol. 63, no. 1, pp. 44–50, Jan. 2025.
- [15] Y. Cheng, C. Huang, W. Peng, M. Debbah, L. Hanzo, and C. Yuen, "Achievable rate optimization of the RIS-aided near-field wideband uplink," *IEEE Trans. Wireless Commun.*, vol. 23, no. 3, pp. 2296–2311, Mar. 2024.
- [16] H. Jiang, W. Shi, Z. Zhang, C. Pan, Q. Wu, F. Shu, R. Liu, Z. Chen, and J. Wang, "Large-scale RIS enabled air-ground channels: Near-field modeling and analysis," *IEEE Trans. Wireless Commun.*, 2024.
- [17] Z. Dong and Y. Zeng, "Near-field spatial correlation for extremely large-scale array communications," *IEEE Commun. Lett.*, vol. 26, no. 7, pp. 1534–1538, Jul. 2022.
- [18] D. Shen, L. Dai, X. Su, and S. Suo, "Multi-beam design for near-field extremely large-scale RIS-aided wireless communications," *IEEE Trans. Green Commun. Netw.*, vol. 7, no. 3, pp. 1542–1553, Sep. 2023.
- [19] S. Lv, Y. Liu, X. Xu, A. Nallanathan, and A. L. Swindlehurst, "RIS-aided near-field mimo communications: Codebook and beam training design," *IEEE Trans. Wireless Commun.*, vol. 23, no. 9, pp. 12 531–12 546, Sep. 2024.
- [20] Q. Yu and L. Dai, "Near-field wideband beamforming for RIS based on fresnel zones," *IEEE Trans. Commun.*, 2024.
- [21] T. T. Bui, T. Q. Do, D. V. Huynh, T. Do-Duy, L. D. Nguyen, T.-V. Cao, V. Sharma, and T. Q. Duong, "Task offloading optimization for UAV-aided NOMA networks with coexistence of near-field and far-field communications," *IEEE Trans. Green Commun. Netw.*, 2024.
- [22] T. Shui, J. Hu, K. Yang, H. Kang, H. Rui, and B. Wang, "Cell-free networking for integrated data and energy transfer: Digital twin based double parameterized DQN for energy sustainability," *IEEE Trans. Wireless Commun.*, vol. 22, no. 11, pp. 8035–8049, Nov. 2023.
- [23] Z. Zhang and Z. Zhao, "Rate maximizations for reconfigurable intelligent surface-aided wireless networks: A unified framework via block minorization-maximization," *arXiv preprint arXiv:2105.02395*, 2021.
- [24] L. D. Nguyen, H. D. Tuan, T. Q. Duong, H. V. Poor, and L. Hanzo, "Energy-efficient multi-cell massive MIMO subject to minimum user-rate constraints," *IEEE Trans. Commun.*, vol. 69, no. 2, pp. 914–928, Feb. 2021.
- [25] D. V. Huynh, S. R. Khosravirad, A. Masaracchia, O. A. Dobre, and T. Q. Duong, "Edge intelligence-based ultra-reliable and low-latency communications for digital twin-enabled metaverse," *IEEE Wireless Commun. Lett.*, vol. 11, no. 8, pp. 1733–1737, Aug. 2022.